Development of a 1K x 1K GaAs QWIP Far IR Imaging Array

M. Jhabvala*[1], K. Choi[2], A. Goldberg[2], A. La[1], S. Gunapala[3],
[1]NASA,Goddard Space Flight Center, Greenbelt, Maryland
[2]Army Research Laboratory, Adelphi, Maryland
[3]Jet Propulsion Laboratory, Pasadena, California

ABSTRACT

In the on-going evolution of GaAs Quantum Well Infrared Photodetectors (QWIPs) we have developed a 1,024 x 1,024 (1K x1K), 8.4-9 μm infrared focal plane array (FPA). This 1 megapixel detector array is a hybrid using the Rockwell TCM 8050 silicon readout integrated circuit (ROIC) bump bonded to a GaAs QWIP array fabricated jointly by engineers at the Goddard Space Flight Center (GSFC) and the Army Research Laboratory (ARL). The finished hybrid is thinned at the Jet Propulsion Lab. Prior to this development the largest format array was a 512 x 640 FPA. We have integrated the 1K x 1K array into an imaging camera system and performed tests over the 40K-90K temperature range achieving BLIP performance at an operating temperature of 76K (f/2 camera system). The GaAs array is relatively easy to fabricate once the superlattice structure of the quantum wells has been defined and grown. The overall arrays costs are currently dominated by the costs associated with the silicon readout since the GaAs array fabrication is based on high yield, well-established GaAs processing capabilities. In this paper we will present the first results of our 1K x 1K QWIP array development including fabrication methodology, test data and our imaging results.

Keywords: Quantum Well Infrared Photodetector, GaAs QWIPs, Infrared Detector Arrays, ROICs.

1. INTRODUCTION

Recently, remarkable advances in the development of GaAs QWIP focal plane arrays have been made. It was only in the late 1980s that single element, angle lapped QWIPs were developed and used[1]. In the 1990s rapid development from single element QWIPs to 512 x 640 arrays[2] occurred across a broad spectrum of the near to far infrared. With the concurrent development of large format silicon readout ICs it has been a relatively simple task for QWIP technology to keep pace. We have recently developed an 8.4-9 μm, 1K x1K QWIP array which was hybridized to a Rockwell Scientific TCM 8050 ROIC. The array was designed jointly by engineers at NASA's Goddard Space Flight Center (GSFC) and the Army Research Laboratory (ARL) and was also jointly fabricated in Goddard's Detector Development Laboratory. Engineers at the Rockwell Science Center in Camarillo, CA performed wafer dicing, indium deposition and hybridization. The hybrid was subsequently thinned at the Jet Propulsion Laboratory (JPL). Testing was performed at both GSFC and the ARL. As with any technological advance we encountered our fair share of hurdles. The design and fabrication of the QWIP arrays was probably the easiest part of the project. However, since the hybridization technology tends to focus on materials other than GaAs we experienced some incompatibilities in the hybridization, thinning and subsequent cooling processes. Thermal incompatibilities caused catastrophic failures of two FPAs, much to our consternation. However, we were able to capture some images before one of the failures and collected data on a third array. Nonetheless, in the space of six months we accomplished the design, fabrication, hybridization and testing of the 1K QWIP array with a minimum budget. One of the advantages of GaAs QWIP technology is the ability to fabricate arrays in a fashion similar to and compatible with silicon IC technology. The designer's ability to easily select the spectral response of the material from 3μm to beyond 15μm is the result of the success of band-gap engineering. The ability to incorporate 2 or more discrete spectral bands[3] onto a single array has been demonstrated in a number of labs and efforts are underway to develop a broadband, 8-14μm, 1K x1K QWIP array[4].

* Murzy.d.Jhabvala@nasa.gov; phone 301 286-5232; fax 301 286-1672; nasa.gov

The applications for QWIP arrays are numerous. At GSFC some of these applications include: studying troposphere and stratosphere temperatures and identifying trace chemicals; tree canopy energy balance measurements; measuring cloud layer emissivities, droplet/particle size, composition and height; SO_2 and aerosol emissions from volcanic eruptions; tracking dust particles (from the Sahara Desert, e.g.); CO_2 absorption; coastal erosion; ocean/river thermal gradients and pollution; analyzing radiometers and other scientific equipment used in obtaining ground truthing and atmospheric data acquisition; ground based astronomy; temperature sounding. Defense and military applications include surveillance, target identification, FLIR, fire control and mine detection[5]. The potential commercial applications are quite diverse. The utility of QWIP arrays in medical instrumentation is well documented[6] and may become one of the most significant QWIP technology drivers. The success of OmniCorder Technologies use of 256 x 256 narrow band QWIP arrays for aiding in the detection of malignant tumors is quite remarkable. Other potential commercial applications for QWIP arrays include: location of forest fires and residual warm spots; location of unwanted vegetation encroachment; monitoring crop health; monitoring food processing contamination[7], ripeness and spoilage; locating power line transformer failures in remote areas; monitoring effluents from industrial operations such as paper mills, mining sites and power plants; IR microscopy; searching for a wide variety of thermal leaks and not least of all; locating new sources of spring water. Recently, F. Freund and his colleagues[8] have been conducting experiments to simulate the effects of the extreme pressures acting on granite cubes to simulate precursor earthquake events. A Goddard built QWIP camera using a Lockheed Martin 256 x 256, 8-8.5 μm, EQWIP [9] was used to detect IR photonic emission during the compressive loading of the granite.

2. QWIP ARRAY DESIGN AND FABRICATION

The design and fabrication of the 1K x 1K QWIP array is straightforward and relatively simple. The architecture of the ROIC determines the pixel pitch which is 18 μm for the Rockwell TCM 8050 ROIC. The spectral response of the detector elements is determined by the quantum well structure, which is grown on semi-insulating GaAs substrate. Since QWIP devices do not respond to normal incidence radiation a method of deflecting the incoming radiation to a direction that is parallel to the wafer surface must be included in the design and fabrication. The ARL has pioneered the technique[10] of corrugating the QWIP array with V-grooves, which reflect normal incidence light 90 degrees into the QWIP.

The QWIP detector structure was modeled and a superlattice growth recipe generated. Fig. 1 shows the calculated peak wavelength λ_p as a function of quantum well width w for different Al molar ratio x in a GaAs/$Al_xGa_{1-x}As$ QWIP structure[11]. Each curve in Fig. 1 is terminated at the well width where the upper state becomes quasi-bound, the point where the detector structure is optimum for high temperature operation. For λ_p = 9 μm, x is chosen to be 0.26 and w is 50 Å. To achieve the desired total quantum well (QW) thickness of 3.5μm, a 62 QW period is needed. Since the corrugated coupling scheme eliminates the need for a grating layer, the top contact GaAs layer can be as thin as 1000 Å. We also included an etch stop layer for substrate removal purposes. The entire growth recipe is shown in Fig. 2.

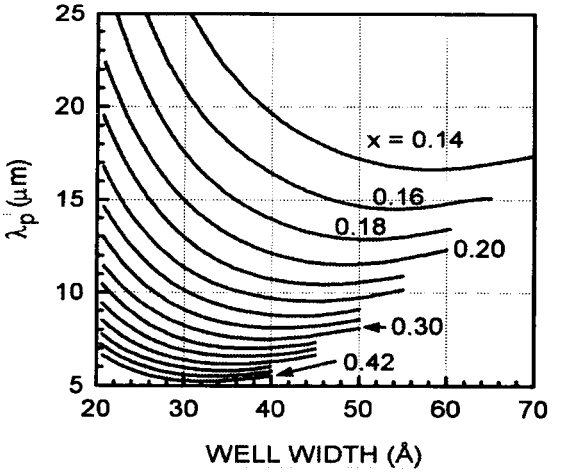

Fig. 1. The calculated detection peak wavelength vs. quantum well width for different values of Al molar ratio.

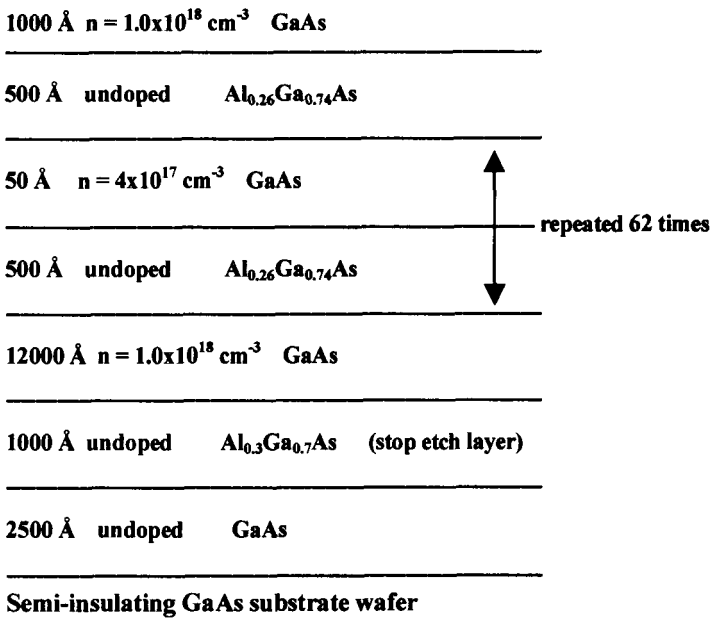

Figure 2. Vertical structure of the detector quantum well. There are approximately 67 layers grown by molecular beam epitaxy.

The pixel geometry design is shown in Fig. 3. The corrugated QWIPs (C-QWIPs) rely on inclined sidewalls to reflect normal incident light into parallel propagation.

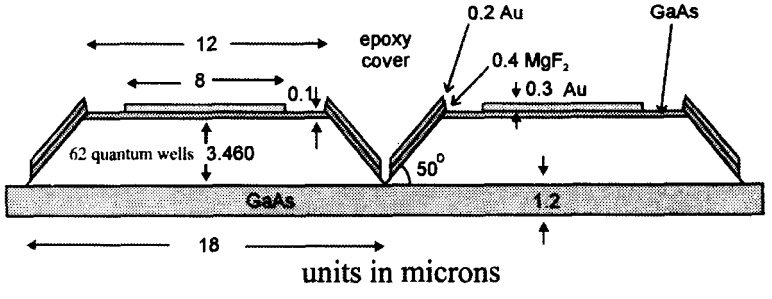

Figure 3. Cross-section of a C-QWIP pixel.

Assuming the angle of the corrugation sidewalls were 45° instead of 50°, the unpolarized external quantum efficiency η, calculated from the decay of light along the optical path, can be expressed as[11]

$$\eta(\alpha, p, t) = \frac{4n}{(1+n)^2}\left\{\frac{1}{p}\left[t + \frac{e^{-\alpha p}}{2\alpha}\left(1 - e^{2\alpha t}\right)\right] + K_0\right\}, \qquad (1)$$

where n = 3.34 (the refractive index of GaAs), p is the corrugation period, t is the height of the corrugations, α is the absorption coefficient the vertically polarized, parallel propagation light, and K_0 is the internal unpolarized quantum efficiency created by the sidewalls at the ends of the corrugations. For infinitely long corrugations, K_0 will be zero, but its value increases with decreasing pixel size. The geometry of a C-QWIP is fixed by the ratio t/p, which is an important structural parameter. Within the 45° sidewall approximation, when t/p = 0.5, the corrugation cross-section is a triangle. When t/p decreases, the corrugation becomes a shallow trapezoid. Detectors with a fixed t/p will have a fixed projection

area fill factor S (=2t/p) available for light reflection i.e. the ratio of the normal incident radiation that is reflected to the total surface incident radiation.

In Fig. 4, η is plotted as a function of p while keeping 2t/p fixed. The value of η increases at first with p because of the larger active volume. But when $t > 1/\alpha$, where $\alpha = 0.22\ \mu m^{-1}$ for typical QWIP materials, most of the light incident under the sidewall is absorbed, η is then limited purely by the fill factor S. For the triangular corrugations (S = 1), the maximum η is 0.5 x 0.71 x S = 0.36, which is half of the unpolarized unit incident power times the transmission coefficient of the substrate. For the trapezoidal corrugation with S = 0.5, the maximum η is 0.18. For a given p, S can be increased by using a thicker active material. In Fig. 4, we show the number of QW periods required to achieve S = 1 for a given p. For example, a p=10 μm triangular corrugation will need 90 QW layers. The value of η can be increased using an anti-reflection coating but was not applied to the present FPAs. Alternatively, η can be increased by thinning the substrate which doubles the optical path length. The value of η thus increases to that with twice the period on the curve representing the same S.

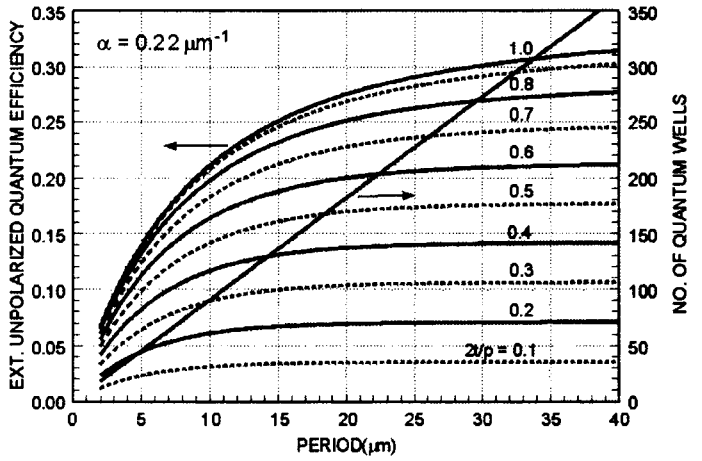

Fig. 4. The theoretical η of C-QWIPs vs. p for $\alpha = 0.22\ \mu m^{-1}$ for different S-values (S=2t/p), assuming $K_0 = 0$ and a thick substrate. The plot also shows the corresponding number of quantum well periods for S = 1, assuming that the thickness of the QW period is 550Å. The value of η for a thinned substrate can be obtained from the same curve at twice the period.

The quantity η in Fig. 4 determines the level of optical absorption, and thus the magnitude of the photocurrent I_p. The noise equivalent temperature difference, NEΔT is determined by the ratio of I_p to the dark current I_d[13]. Hence, the detection sensitivity depends on η/I_d rather than η alone. Furthermore, background limited performance BLIP is achieved only when $I_p > I_d$. Due to the reduced active volume in C-QWIPs, I_d is reduced by a factor (p–t)/p = (1–S/2). Therefore, when comparing with other couplings that have no dark current reduction, as with a grating, a new quantity η' is defined, where

$$\eta' \equiv \eta \frac{I_d(45)}{I_d} = \eta \frac{p}{p-t} = \frac{\eta}{1-S/2}. \qquad (2)$$

The value of η' is the quantum efficiency normalized to the full geometrical dark current. We should however emphasize that η' is not a valid figure of merit when comparing different material technologies. Fig. 5 shows the values of η' for the same detector parameters as in figure 4. From figure 5, it is evident that the dark current reduction further enhances the performance of C-QWIPs with large S, and η' is maximized at fixed t when S = 1. Fig. 5 shows that the effective C-QWIP quantum efficiency can be larger than 50%. In comparison, grating couplings typically have η' (=η) of 10%.

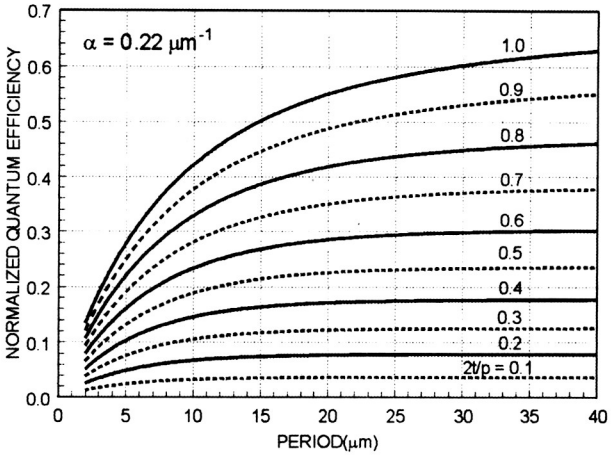

Fig. 5. The theoretical η' of C-QWIPs vs. p for $\alpha = 0.22\ \mu m^{-1}$ for different S = 2t/p, under the geometrical model with $K_0 = 0$ and thick substrate. The value of η for thinned substrate can be similarly read off from the same curve at twice the period.

An advantage of the corrugated coupling scheme is its scalability to small pixel sizes. In the present 1024 x 1024 FPA, the pixel area is 18 μm x 18 μm. One can choose t = 3 μm and p = 6 μm for 3 corrugations per pixel, Fig. 4 shows η will be 16% for an unthinned substrate and 23% for a thinned substrate. If we increase t to 9 μm and utilize 1 corrugation per pixel, then ηincreases to 27% for the unthinned device and to 31% for the thinned device. The corresponding η' will be 54 and 62%, respectively. These two examples illustrate the improvement in performance that can be achieved with larger triangular corrugations. However, 9 μm is too thick to be compatible with the wafer fabrication process. We selected t = 3.5 μm and p = 18 μm for the present one corrugation per pixel design. From Figs. 4 and 5, η for this FPA (S = 0.39) will be 13% (unthinned substrate) and 14% (thinned substrate) and η' = 17% (thinned substrate). Although these η and η' are 2.2 and 3.6 times respectively smaller than that of the t = 9 μm detector, the simplicity of the processing steps and the moderate material thickness made it a good starting point for the initial demonstration of this large format FPA.

Fig. 6 shows the actual mesa sidewall profiles of the FPA pixels in the two orthogonal directions. These mesas are created by wet etching through a square mesa mask. Under this approach, there is undercut in one of the directions, which significantly shortens the length of the corrugations and reduces the material fill factor. It is this undercutting which makes it infeasible to produce a viable 9 μm thick triangular corrugation with a single chemical etching. When one etches 9 μm into the material, the undercut in the other direction will eliminate the majority of the active material. However, as seen in Fig. 6, it is unnecessary to utilize such a thick material since the non-vertical sidewalls at the ends of the corrugations will also contribute to light reflection thus making K_0 large. This additional sidewall reflection compensates the relatively small S in this pixel design.

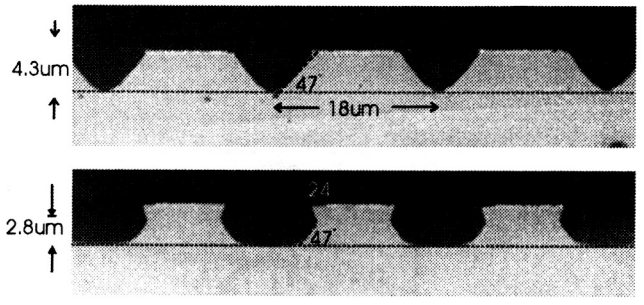

Fig. 6. The pixel mesa profiles in two orthogonal directions, the top figure shows the regular corrugated sidewalls and the bottom figure shows the hour-glass sidewalls. Each corrugation period represents one pixel. The pixels in this particular wafer are slightly over etched from its designated value of 3.6 μm, but this over-etch will not affect the detector operation.

Our numerical analysis modeling predicts the quantum efficiency of the hour-glass sidewalls, η_H to be 10% for both the thinned and unthinned devices, which is to be expected from the fraction of the properly inclined sidewalls. The total combined η from both sets of sidewalls is 15% unthinned and 20% thinned. These values of η have taken the smaller material fill factor into account and are calculated from $f_x\eta_C + f_y\eta_H$, where f_x and f_y are the material fill factors in each direction respectively and η_C is the quantum efficiency of the regular corrugated sidewalls. Since the remaining active volume is 37% of the original volume, there is a correspondingly less dark current. The value of η' is then equal to 40% unthinned and 54% thinned. This level of performance is comparable to that with the 9 μm tall corrugations even though the actual superlattice thickness is a manageable 3.6 μm.

Our QWIP array fabrication process requires three masks for: 1) the detector mesa formation; 2) the ohmic metal pixel contacts and; 3) the insulator/reflector layer definition. The process begins with a wafer cleaning procedure followed by photoresist deposition and the exposure of the mesa definition mask. A phosphoric / peroxide acid etches the GaAs mesas. The second masking step defines the lift-off areas of deposited Ge/Au/Ag/Au metal followed by a rapid thermal anneal. The third mask step defines the areas for the lifting off the insulator and sidewall metal reflector. This sidewall reflector is mainly to prevent possible infrared absorption in the epoxy through the fringing optical field. This third step can be eliminated depending on the epoxy backfill requirement of the subsequent hybridization process. The entire QWIP wafer fabrication process can be completed in less than 4 days. Five complete 1K x 1K die were fabricated on a single 3-inch wafer but 4-inch diameter wafers are just as available. After fabrication we performed some diagnostic tests and then sent the wafer to Rockwell Science Center for the hybridization process. Indium bumps are applied, the wafer is diced and candidates are bump bonded to the silicon readout. The hybrids were either packaged in an LCC or sent to JPL for further thinning. In order to test the detector characteristics in a single detector format, we also processed a wafer with the same QW specifications except that the number of QW periods was 40 instead of 62. This test wafer was processed into large area C-QWIPs with a corrugation period of 8.5 μm.

The 1K x 1K die was bump bonded to Rockwell's TCM 8050 ROIC[14]. The characteristics of this particular ROIC are identified in Table 1. This is one of the only readouts available with an adequate full well capacity for high background applications. Most very large format readouts are intended for low background, astronomical applications where the number of available photons is generally small.

TABLE 1. Characteristics of the Rockwell TCM 8050 ROIC.

Array Format	1,024 x1,024
Pixel size	18μm x18μm
Number of video outputs	4
Full well capacity	3 million electrons
Max pixel rate	20 MHz/channel
Conversion gain	selectable from 0.34 μv/e- to 2.7 μv/e-
Read noise	<300 electrons
Power dissipation	<150 mW
Cold operating temperature	below 70K

Shown below in Fig. 7 are two images. The first is an image of a section of the QWIP wafer surface showing the pixels and substrate contacts. The second photograph shows the mounted 1K x 1K QWIP hybrid in an LCC package.

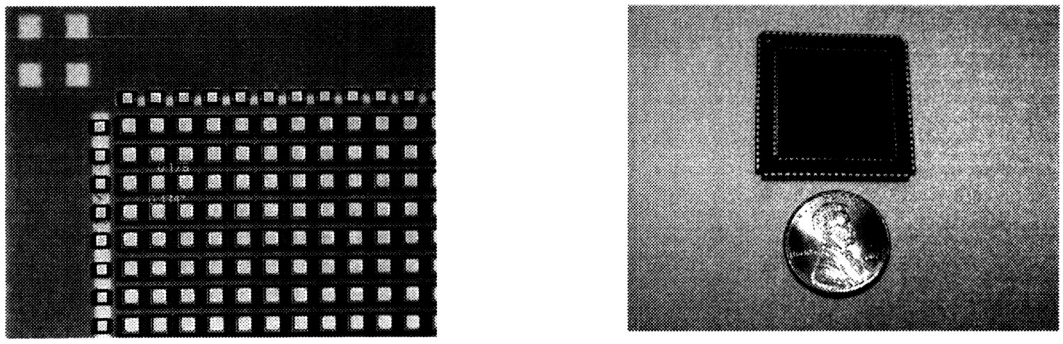

Figure 7. Photomicrograph of QWIP array corner of about 90 pixels (left) and photograph of QWIP hybrid in an LCC (right).

3. EXPERIMENTAL RESULTS

The mean spectral response of the detectors in the FPA was measured by imaging the output slit of a grating monochromater (Optronics Laboratories OL750) onto the FPA and collecting images of the monochromatic light from 7-10 μm at 0.1 μm intervals. The spectral response was measured at a bias of –1 V and an operating temperature T= 65K. The result is shown in Fig. 8. In addition, the large area test sample was characterized in another system with an equivalent applied bias of –3 V and T=10 K. The slight difference between the two detectors can be due to the differences in the measuring systems, the wafer materials and the applied bias. Overall, the detection peaks of 8.7 and 8.9 μm agree with the designed peak of 9 μm in Fig. 1.

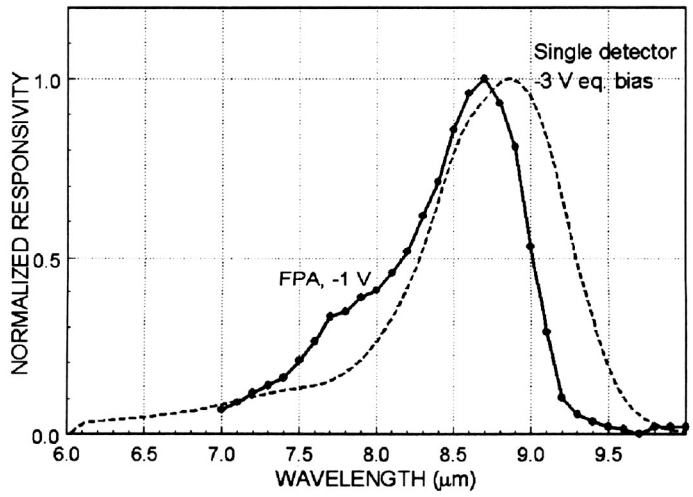

Fig. 8. Spectral response of C-QWIP single detector and FPA.

Fig. 9 shows the 77 K dark current, I_d, of the large area detector and also the 293 K background generated signal photocurrent I_p measured at T = 10 K (well out of range of dark current generation). The currents have been scaled to an 18 μm x 18 μm pixel. This C-QWIP shows I_p slightly less than I_d with refractive optics (f/1.5) at 77 K. In this high background environment, we note that at an operating temperature of 76K the signal current from the 293K background is equal to the QWIP dark current and we take this to be the BLIP condition.

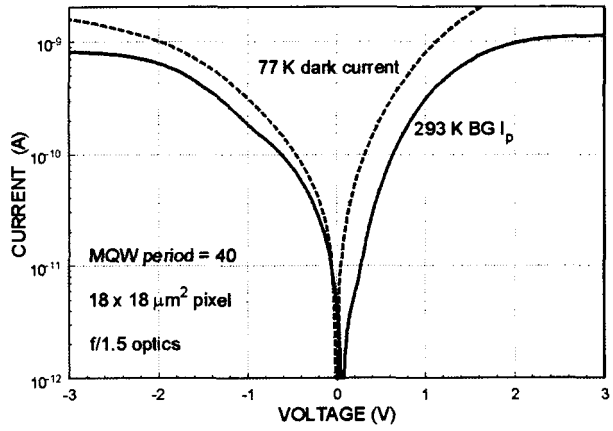

Fig. 9. The dark current and the photocurrent of a C-QWIP with corrugation period = 8.5 μm.

The first two FPAs we fabricated were not thinned. The first FPA which was used to measure the spectral response failed mechanically (shattered) after only three thermal cycles before we could accurately measure the dark current and responsivity. The second FPA we tested had a defect in the ROIC that prevented us from adjusting the integration time. The integration time was slaved to the frame rate and as result was a fixed 50 ms. In order to avoid saturation of the ROIC charge well, we had to decrease the bias on the detector to –0.1 V. Nevertheless, we were able to observe that the dark current and photocurrent were approximately equal at 75 K and we were able to acquire a number of 1024 x 512 laboratory images. Fig. 10 shows the pixel total current I_{tot} as a function of temperature under a 293 K background. Over the range of temperatures we tested the FPA, the decrease of I_{tot} is significantly slower than that estimated from the activation energy of the dark current. Therefore, the detection is near the QWIP BLIP limit at a temperature as high as 76K, similar to the test sample. This result indicates that the light coupling is not affected by the small S design. The level of I_{tot} of the FPA is consistent with $I_p + I_d$ of the test detector for the same equivalent bias.

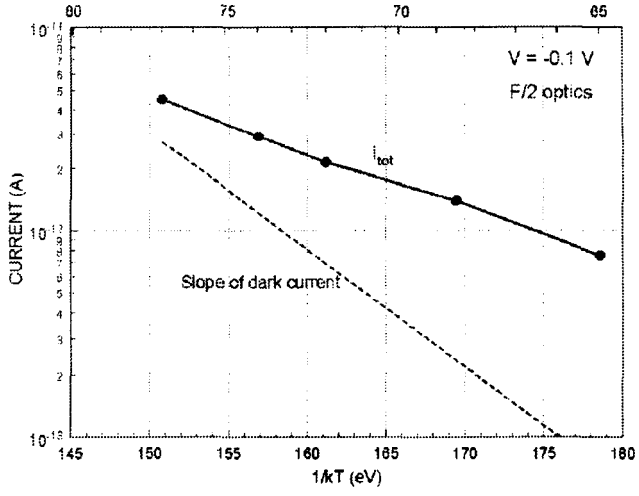

Fig. 10. The pixel total current from a constant background of 293 K.

The near BLIP performance is supported by the high quality infrared imageries taken over this temperature range. Four images (f/2) are shown in Fig. 11 taken with the FPA at 77K, 74K and 65K. There is a slight improvement before signal

processing between the 77K images we collected and the 74K images. The further improvement displayed in the two images taken at 65K are a result of a combination of factors including refined optical focusing and a higher pre-amp gain. We were severely constrained by the inability to adjust the integration time and some excess system noise.

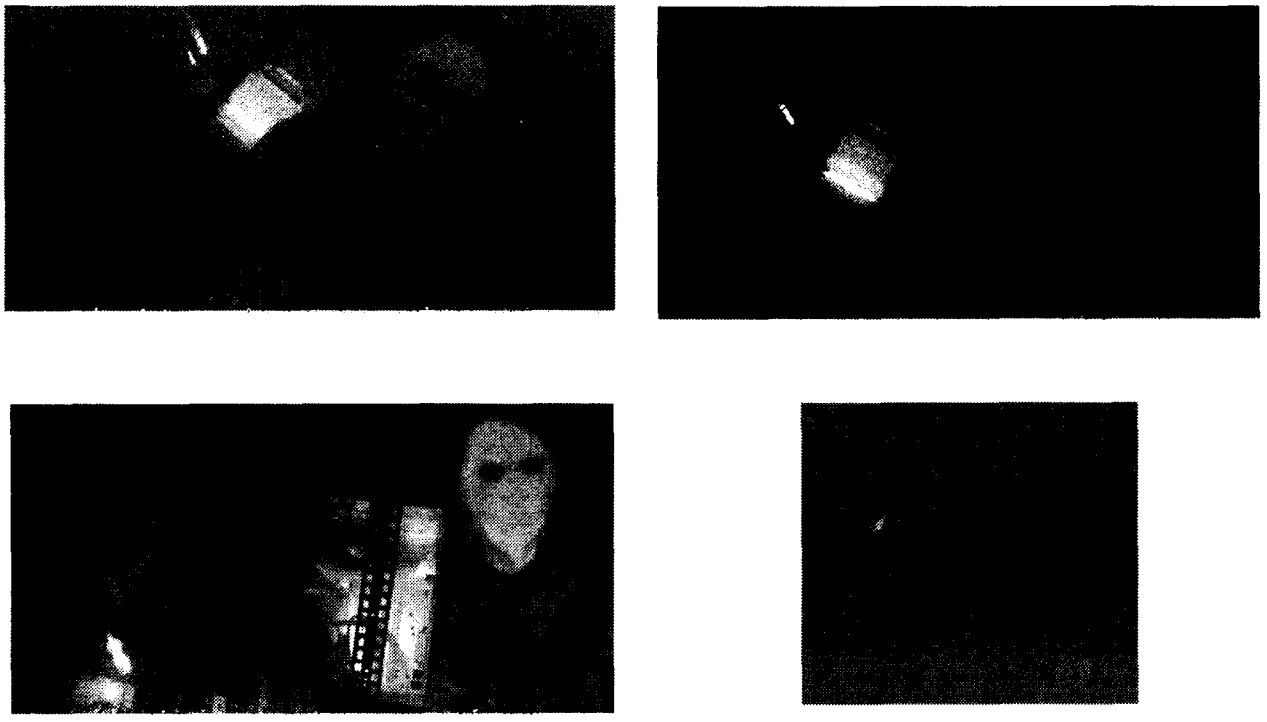

Fig. 11. Images acquired with the 8.4-9μm, 1K x 1K QWIP array. Top left: two-quadrant (512 x1K) image with the FPA temperature, T, at 77K: Top right; the same image with T=74K: Bottom left; two-quadrant image of engineers and an exposed computer CPU: Bottom right; high-resolution image of a heated soldering iron tip, T=65K in both bottom images.

4. FUTURE WORK

We have, up to this point, successfully developed three generations of QWIP arrays starting with the development of a 128 x 128 array[15] a 256 x 256 array and recently a 640 x 512, four-color array[3]. We have encountered little or no difficulty in the hybridization of the GaAs to the appropriate ROIC. This is largely due to the fact that we were following in the footsteps of the technology pioneered in the development of HgCdTe arrays. However, in the hybridization of this array and the subsequent thermal cycling during testing we encountered a number of catastrophic failures. The QWIP arrays are relatively inexpensive and can be quite plentiful with high yield but this is not the case for large format, science grade ROICs and hybridization. In the immediate future we will solve our thermal mismatch problems and fabricate new arrays and hybrids. Our test data was acquired from QWIP arrays that were unthinned which compromises the performance of the device. Future arrays will be thinned which requires an undesirable a break in the hybridization process.

The Rockwell ROIC has a pixel pitch of 18μm. We are exploring another ROIC that will have a larger pitch, on the order of 25μm. With both of these options available we intend to build additional narrow band QWIP arrays for a variety of applications as mentioned earlier. We are also funded by the NASA Earth Science Technology Office (ESTO) grant to develop an 8-14μm, 1K x 1K array as part of the Advanced Component Technology program. We are continuing to refine the GaAs fabrication process to improve a number of process related performance factors such as quantum efficiency, optical collection efficiency and excess dark current. The array uniformity and 1/f noise are

intrinsically well behaved so QWIP improvements can be made at the materials and processing levels. With the current advancement of mechanical cryocoolers[16] operating far IR QWIP arrays without cryogen is rapidly becoming commonplace further simplifying new system implementation.

5. SUMMARY

We have successfully developed and operated a 1,024 x 1,024 GaAs QWIP array. The design, fabrication, hybridization and testing were accomplished through a highly collaborative effort between Goddard, the Army Research Lab, JPL and Rockwell with each group contributing their own particular technological expertise. Even though the effort is the culmination of many years of QWIP research and development, we as a group were able to develop this device with minimal funding and in a very short span of time. The ease of fabrication, the relatively high device yield, the compatibility with existing silicon processing techniques and the compatibility with a variety of available readout ICs make QWIP technology very attractive for many applications. We expect that after refining our fabrication techniques that arrays sensitive in the near to far IR with a tunable bandwidth will be routinely available. Performance of these arrays will be comparable to any existing QWIP devices (e.g. NEΔT < 10mK in the 7-9μm band). As with any new development we encountered some hurdles which limited our current capabilities but which are easily, (and will be) remedied. Specifically, we need to refine our packaging technique to minimize thermal effects. Our initial results indicate we have solved this problem but at great expense to our initial inventory of five devices. The remaining one array has a readout defect which limits our testing ability. We are currently fabricating an additional lot of devices which will use the same Rockwell TCM 8050 ROIC. We are intending to pursue the development of a 2K x 2K array but the limitation is the readout availability and cost. Manufacturing the detector is straightforward.

ACKNOWLEDGEMENTS

This work was supported by the Directors Discretionary Fund of the Goddard Space Flight Center. We would like to express our gratitude to K. Vural, S. Wong and the overall support we received from the Rockwell Science Center. We are also grateful for the efforts of J. Liu of the JPL and the support of B. Ottens of the GSFC.

REFERENCES

1. B. F. Levine, C. Bethea, G. Hasnian, V. Shen, E. Pelve, R. Abbott and S. Hsieh, *Appl. Phys. Lett.* v.56, pp. 851-853, 1990.

2. H. Schneider, P. Koidl, M. Walther, J. Fleissner, R. Rehm, E. Diwo, K. Schwarz and G. Weimann, *Infrared Physics and Technology*, v 42, pp283-289, 2001.

3. M. Jhabvala, S. Gunapala, D. Reuter, K. K. Choi, S. Bandara, J. Liu, A. La, S. Banks, J. Cho, T. Hwang, S. Tsay, D. Rafol, H. Huet, N.Chauvet and T. Huss, *Infrared Physics and Technology,* to be published 2003.

4. M. Jhabvala, S. Gunapala, D. Reuter, K. K. Choi and S. Tsay, NASA Earth Science Technology Office *Advanced Component Technology* proposal award, 2003.

5. A. Goldberg, K. Choi, M. Jhabvala, A. La, P. Uppal and M. Winn, to be published in *Proceedings of SPIE*, Orlando, 2003.

6. M. Fauci, R. Breiter, W. Cabanski, W. Fick, R. Koch, J. Ziegler and S. Gunapala, *Infrared Physics and Technology*, Vol. 42, pp 337-344 June, 2000.

7. R. Gaughan, *Biophotonics International*, pp 20-21, March, 2003.

8. F. Freund, private communication.

9. P. Mitra, A. Brouns, F. Case and J. McCurdy, *SPIE Conference 4820*, July, 2002.

10. A. Goldberg, K. Choi, N. Das, A. La, M. Jhabvala, R. Bailey and K. Vural, *Proceedings of the 1999 IRIS Speciality Group Meeting on Detectors*, ERIM, 1999.

11. K. K. Choi, *J. Appl. Phys.* **73**, 5230 (1993).

12. K. K. Choi, C. J. Chen and D. C. Tsui, *J. Appl. Phys.* **88**, 1612 (2000).

13. K. K. Choi, C. J. Chen, A. C. Goldberg, W. H. Chang, and D. C. Tsui, *SPIE* **3379**, 441 (1998)

14. rsc.rockwell.com/imaging/ROIC_Ref_Table.html on the World Wide Web.

15. M. Jhabvala, K. Forrest and R. Kaipa, *Technology 2001*, San Jose, CA, Dec 3-5, 1991

16. sunpower.com on the World Wide Web.